



## Manuscript Information

**Journal name:** Nuclear instruments & methods in physics research. Section A, Accelerators, spectrometers, detectors and associated equipment

**NIHMSID:** NIHMS375866

**Manuscript Title:** Development of a Head Scanner for Proton CT

**Principal Investigator:**

**Submitter:** Author support, Elsevier (m.ridder@elsevier.com)

## Grant/Project/Contract/Support Information

Name	Support ID#	Title
------	-------------	-------

## Manuscript Files

Type	Fig/Table #	Filename	Size	Uploaded
manuscript		NIMA_54382.pdf	797571	2012-05-08 09:09:39
citation		375866_cit.cit	164	2012-05-08 09:09:38

This PDF receipt will only be used as the basis for generating PubMed Central (PMC) documents. PMC documents will be made available for review after conversion (approx. 2-3 weeks time). Any corrections that need to be made will be done at that time. No materials will be released to PMC without the approval of an author. Only the PMC documents will appear on PubMed Central -- this PDF Receipt will not appear on PubMed Central.

## Accepted Manuscript

Title: Development of a Head Scanner for Proton CT

Authors: H.F.-W. Sadrozinski, R.P. Johnson, S. Macafee, A. Plumb, D. Steinberg, A. Zatserklyaniy, V. Bashkirov, F. Hurley, R. Schulte

PII: S0168-9002(12)00384-1  
DOI: 10.1016/j.nima.2012.04.029  
Reference: NIMA/54382

Published in: *Nuclear Inst. and Methods in Physics Research, A*

Received date: 28 January 2012

Revised date: 6 April 2012

Accepted date: 9 April 2012

Cite this article as: Sadrozinski HF-W, Johnson RP, Macafee S, Plumb A, Steinberg D, Zatserklyaniy A, Bashkirov V, Hurley F, Schulte R, Development of a Head Scanner for Proton CT, *Nuclear Inst. and Methods in Physics Research, A*, doi:10.1016/j.nima.2012.04.029

This is a PDF file of an unedited manuscript that has been accepted for publication. As a service to our customers we are providing this early version of the manuscript. The manuscript will undergo copyediting, typesetting, and review of the resulting proof before it is published in its final citable form. Please note that during the production process errors may be discovered which could affect the content, and all legal disclaimers that apply to the journal pertain.

© 2012 Elsevier B.V. All rights reserved.

# Development of a Head Scanner for Proton CT

H. F.-W. Sadrozinski\*, R. P. Johnson, S. Macafee, A. Plumb, D. Steinberg, A. Zatserklyaniy  
*Santa Cruz Institute for Particle Physics, UC Santa Cruz, Santa Cruz, CA 95064, USA*  
V. Bashkirov, F. Hurley, R. Schulte  
*Loma Linda University Medical Center, Loma Linda, CA 92354, USA*

*Abstract*– We describe a new head scanner developed for Proton Computed Tomography (pCT) in support of proton therapy treatment planning, aiming at reconstructing an accurate map of the stopping power (S.P.) in a phantom and, in the future, in patients. The system consists of two silicon telescopes which track the proton before and after the phantom/patient, and an energy detector which measures the residual energy or range of the proton to reconstruct the Water Equivalent Path Length (WEPL) in the phantom. Based on the experience of the existing prototype and extensive Geant4 simulations and CT reconstructions, the new pCT scanner will support clinically useful proton fluxes.

PACS: 29.40.Gx, 29.40.Vj, 29.40.Wk, 87.55.Gh, 87.55.K-, 87.57.Q-

Keywords: Proton CT, Proton treatment planning, Head scanner, Silicon strip detector, Range counter, SiPM.

## 1 INTRODUCTION

Proton therapy and treatment planning requires the knowledge of the stopping power (S.P.) in the patient, such that by tuning the proton energy, the Bragg peak can be located within the tumor. The goal of Proton CT (pCT) is to reconstruct a 3D map of the S.P. by measuring the residual range of protons of higher energy than those stopping in the patient. We presented the requirements for pCT in 2002 [1], and proposed in 2003 a detector system [2], which incorporated the basic building blocks of a pCT system: a tracker to measure the proton path before and after the phantom, and allows to calculate the Most Likely Path (MLP) the proton has taken within the phantom [3], and an energy detector to measure the residual energy or range of the proton, which is used to calculate the Water Equivalent Path Length (WEPL) in the phantom.

Since Multiple Coulomb Scattering (MCS) is a major issue to the spatial precision of the localization of the proton path, we confirmed in a beam test that the path inside a phantom can be predicted with sub-mm precision using external tracking and the MLP formalism [4]. We have constructed a prototype scanner based on detector technology developed in High Energy Physics (silicon strip sensors and CsI hodoscopic calorimeter) [5], and it is now used to develop methods for calibrating the instrument in terms of WEPL and to refine image reconstruction methods [6]. In the following we describe a new pCT head scanner now under construction which will allow data taking at speeds required for clinical application, and which is expected to minimize the needs for detector calibration and data corrections. In Section 2 we present its design, layout and principle of operation, which are based on lessons learned from the existing detector and extensive Geant4 simulations. Section 3 has details of the research on the silicon tracking system, and Section 4 describes the on-going work on the energy detector.

## 2 DESIGN OF THE PCT HEAD SCANNER

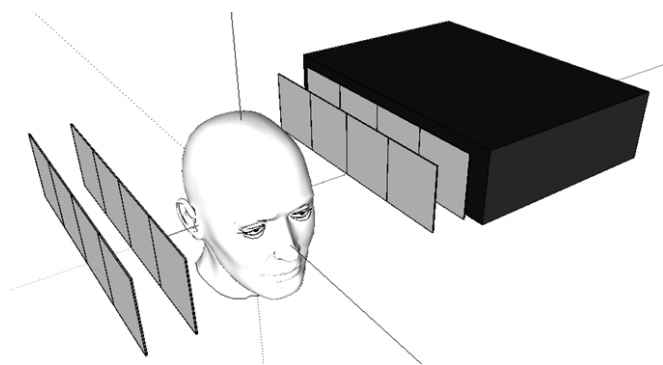
The requirement that the MLP and the integrated S.P. be determined for every proton presents an instrumental challenge due to the large amount of data needed for pCT. To reconstruct the 3D S.P. map, 2D images are taken in a rotational scan with typical 2 degree steps (e.g. about the vertical axis in Fig. 1). For each of these 180 “views, one needs to have sufficient proton histories in each 1 mm<sup>3</sup> voxel to reliably determine the contribution of that voxel to the integrated S.P. The number of required protons has been

---

\*Corresponding author, hartmut@scipp.ucsc.edu, Tel: (831) 459 4670, Fax:(831) 459 5777

1 estimated in Refs. [7] and [8], where the image quality was compared to the number of proton histories in  
 2 the voxels. Stable solutions were found with 25 proton histories. Taking into account the loss of protons  
 3 due to non-ionizing interactions in the phantom (~50%) and an additional loss of 50% in the fitting  
 4 procedure for the most probable value in the residual energy, we find that we need 100 protons for every  
 5  $1\text{mm}^3$  voxel in each of the 180 views, which requires  $\sim 7 \cdot 10^8$  protons for a head-size object. With 10 kHz  
 6 data rate, which is the data acquisition speed of our prototype scanner [5], one pCT scan will take 20 hrs,  
 7 while a scan with a proton rate of 2 MHz will take 6 min. Our key specification is that proton histories can  
 8 be acquired at a sustained 2 MHz rate to permit clinical application. Progress in data analysis might allow  
 9 us to fit the entire residual energy spectrum instead of just the end-point, reducing the required number of  
 10 proton histories, the needed scan time.

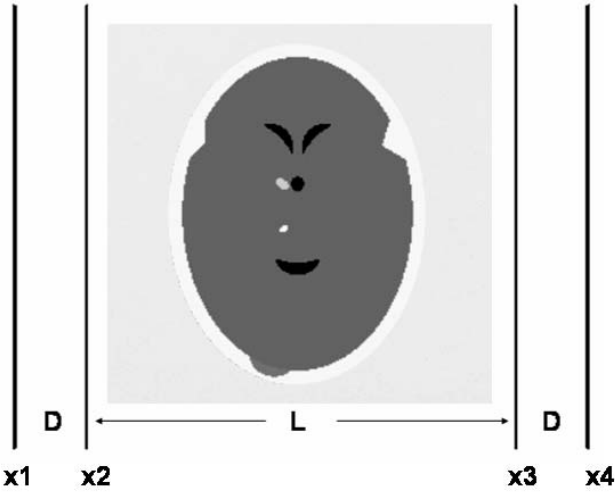
11 Figure 1 shows the layout of the head scanner. Protons with kinetic energy of 200 MeV coming from the  
 12 left encounter the entrance telescope, the phantom, the exit telescope and are stopped in the energy  
 13 detector/range counter. The entrance and exit telescopes each consist of two x-y planes of silicon sensors to  
 14 allow the extrapolation of the proton trajectory into the phantom. The head phantom is mounted on a stage  
 15 which can be rotated through a vertical axis. Not shown are the accelerator window and a scattering foil  
 16 which enlarges the beam, about 200 cm upstream from the center of the phantom.  
 17



18 **Fig. 1. Layout of the pCT head scanner under construction. A proton entering from the left is first tracked in**  
 19 **the entrance telescope of two x-y planes of silicon strip sensors, and after passing through the**  
 20 **phantom/patient, in the similarly constructed exit telescope, before its residual energy/range is determined in**  
 21 **the energy detector.**  
 22  
 23

24 The desire to image a large volume of the head determines the lateral dimensions of the scanner. The  
 25 aspect ratio is given by the goal to reconstruct a limited number of vertical “slices” of the 3D S.P. map,  
 26 while the entire width of the head has to be covered in all “views”. The active area is 9 cm high and 36 cm  
 27 wide, allowing the use of silicon sensors from 6” wafers as shown in Figs. 1 and 4.

28 An important design criterion for the scanner is compactness to reduce interferences within the gantry  
 29 area. This means that all distances along the proton path should be minimized whenever possible. Using  
 30 high-precision silicon sensors allows reducing the sensor separation  $D$  in the entrance and exit telescopes,  
 31 (see Fig. 2), and is set to  $D = 5$  cm, as discussed in more detail in Sec. 3.3. The distance  $L$  between  
 32 entrance (front) and exit (back) telescope is a critical parameter, and has been investigated with GEANT4  
 33 simulations of a Herman head phantom [9], followed by reconstruction [6] of the relative stopping power  
 34 (RSP), which is the S.P. relative to water.



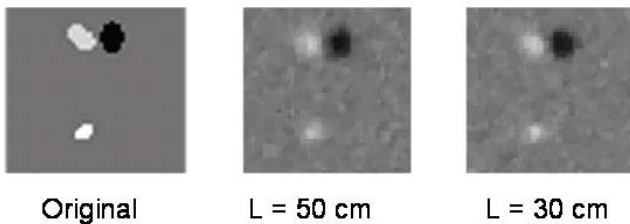
1  
2 **Fig. 2. Critical tracker distances for simulations with a Herman head phantom [9]. L is the distance between**  
3 **front and back telescopes and D is the intra-telescope distance between the pair of x-y planes, taken to be the**  
4 **same in both front and back.**

5  
6 In Fig. 3, we clearly see a difference in the reconstructed images from simulations with  $L=50$  cm and 30  
7 cm. To quantify the image quality, we introduce the reconstruction error  $\sigma_{\text{Rec}}$  as a measure of the goodness  
8 of the reconstruction:

$$9 \quad \sigma_{\text{Rec}} = \sqrt{\sum_{\text{Voxels}} \{RSP_i(\text{reconstructed}) - RSP_i(\text{phantom})\}^2},$$

10 where we add in quadrature the RSP differences in the voxels. When we extend the sum over the entire  
11 phantom, which has large areas with homogeneous RSP, we find  $\sigma_{\text{Rec}} = 16.22$  for  $L = 50$  cm and  $\sigma_{\text{Rec}} =$   
12  $15.42$  for  $L = 30$  cm. Selecting a 20 pixel x 20 pixel area around the white spot in the bottom center of Fig.  
13 3, where the reconstruction accuracy depends on the spatial resolution, we find a much larger relative  
14 difference with  $\sigma_{\text{Rec}} = 0.53$  for  $L = 50$  cm and  $\sigma_{\text{Rec}} = 0.31$  for  $L = 30$  cm. Thus we set the distance L to  
15 the minimum distance permitting free rotation of the phantom,  $L = 30$  cm.

16 The depth of the energy detector is 30 cm of water equivalent thickness (WET), sufficient to stop 200 MeV  
17 protons.



19  
20 **Fig. 3. Original and pCT reconstruction of a Herman head detail [9] simulated with two distances between**  
21 **front and back telescope: L= 50 and 30 cm.**

### 23 3 TRACKER DESIGN AND R&D

24 The tracker has to measure the proton path with sufficient precision to allow the reconstruction of the  
25 MLP with sub-mm accuracy within the phantom. The sensors need to be fast, thin to limit MCS, and have  
26 fine pitch.

### 3.1 Silicon Sensors

Silicon strip sensors are an attractive choice since they have low noise at good efficiency, an important factor in a sparse system with no redundant space points. We will use single-sided silicon strip detectors (SSD) developed for the Fermi mission manufactured by Hamamatsu Photonics [10], with sensors with horizontal and vertical strips mounted back-to-back on printed circuit boards. In order to cover the active area, the sensors with 228  $\mu\text{m}$  pitch from 6" wafers will be tiled as shown in Fig. 4. SSDs with vertical strips are read out individually, while those with horizontal strips are bonded together in pairs and read out at the end.

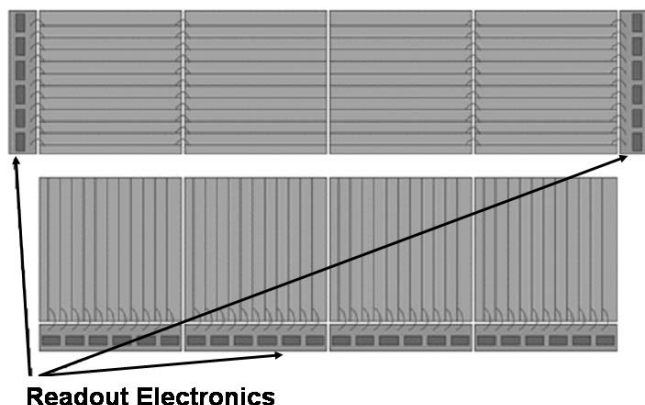


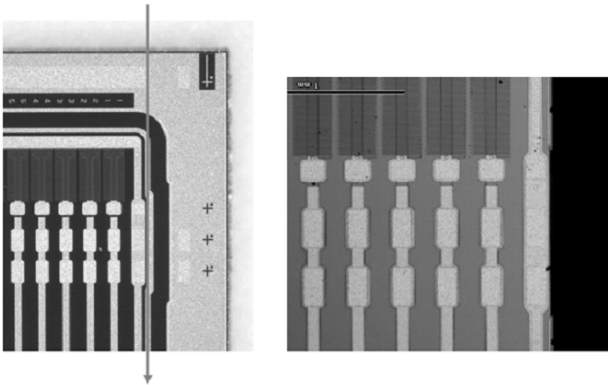
**Fig. 4. Layout of one x-y tracking planes of 6" silicon strip sensors, showing the two back-to-back sides separately, indicating the location of wire bonds and readout electronics. Pairs of sensors with horizontal strips are wire bonded together and read out at the ends.**

### 3.2 Slim Edges

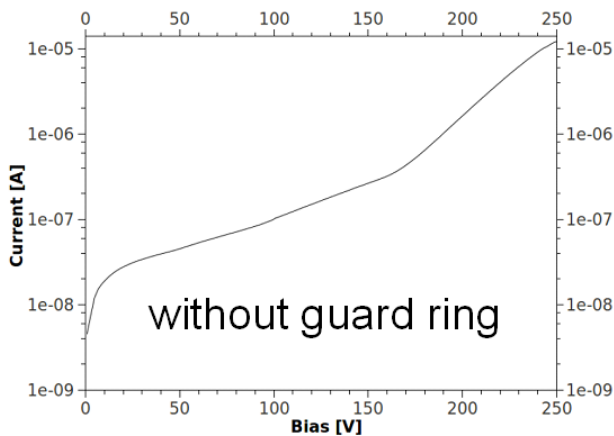
One issue is that the wafer sizes are limited to 6" and that the active area of the sensors is surrounded by a 1 mm wide dead edge area, which prevents seamless tiling. In the prototype described in Ref. [5] the sensors were overlapped by 5 mm to have 100% coverage, which led to artifacts in the reconstructed images, when not taken into account properly. To avoid having to correct for this variation in effective sensor thickness, we are developing "slim edges" on Si sensors which will allow tiling without overlap and minimal dead area [11]. This is done in collaboration with the US Naval Research Lab (NRL). Slim edges can be fabricated on finished sensors in a "scribe-cleave-passivate" (SCP) treatment involving Laser +  $\text{XeF}_2$  scribing, followed by cleaving and passivation of the edge with plasma-enhanced chemical-vapor-deposited (PECVD) nitride for n-type and atomic-layer-deposited ALD with alumina for p-type sensors. Details of the treatment are given in Ref. [11]. Pictures of a Fermi "Baby" detector [10] before treatment and with a slim edge without a guard ring, respectively, are shown in Fig. 5.

Figure 6 shows the total detector currents for the slim edge sensor of Fig. 5, which has an edge length of 3.5 cm, an area of 5.6  $\text{cm}^2$  and a thickness of 400  $\mu\text{m}$ . At the depletion voltage of 100V, the currents are less than 100 nA when the guard ring is cut away as shown in Fig. 5 and less than 10 nA when the cut is outside the guard ring (not shown). Individual strip currents before and after cutting are essentially unchanged. In addition, we have found that the charge collection on the strips next to the slim edge is unchanged when compared to before cleaving [12]. Up to now, about 50 test structures with edge length up to 10 cm have been treated successfully with distances down to 14  $\mu\text{m}$  between active area and edge. For the existing Fermi sensors [10] with fairly large distances between implants (see Fig. 5), our process permits reducing the width of the dead edge area from 1 mm to less than 200  $\mu\text{m}$ . The next step is

1 extending the cleaving from the test structures to the full size sensors, for which industrial methods will be  
 2 used.



3  
 4 **Fig. 5.** Generating a “slim” edge of less than 250  $\mu\text{m}$  on a Fermi p-on-n “Baby” sensor [10]. The corner of  
 5 the untreated sensor is shown on the left, with the planned cut between bias line and guard ring indicated by  
 6 the vertical line. The SCP treated sensor is shown on the right, with the strips and the bias ring visible, but no  
 7 guard ring. The strip pitch is 228  $\mu\text{m}$ .  
 8

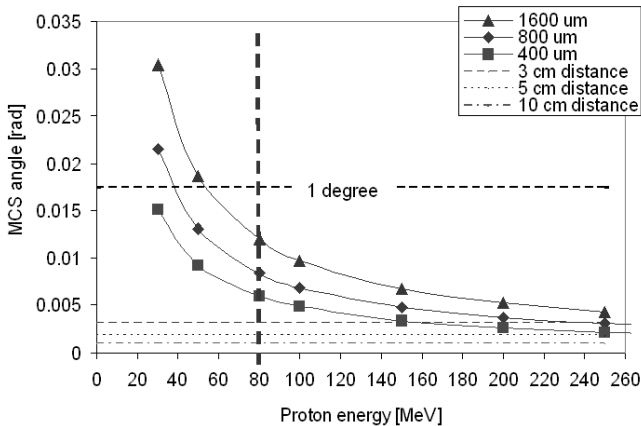


9  
 10 **Fig. 6.** The I-V curve of a Fermi “Baby” after SCP treatment cleaving away the guard ring shows a leakage  
 11 current of less than 100 nA at the operating voltage of 100 V.  
 12

### 13 3.3 Silicon Sensors Thickness

14 The thickness of the silicon sensors plays a role in tracking since the multiple scattering MCS reduces the  
 15 accuracy with which proton tracks can be extrapolated into the phantom. From Fig. 2 one can understand  
 16 that large MCS angles in the front detector x2 and the back detector x3 will go undetected and will distort  
 17 the MLP determination. This is especially important for the protons traversing the phantom not at the  
 18 center where the multiple scattering in the phantom is maximal and the extrapolation distance is smallest,  
 19 but at larger lateral distances where the multiple scattering in the phantom is reduced and the extrapolation  
 20 distance is larger. In that case, a more accurate determination of the entrance and exit location will improve  
 21 the MLP calculation. Figure 7 shows a comparison between the MCS angle in one x-y plane (calculated  
 22 according to Moliere’s approximation) with the intrinsic resolution of the telescope due to the sensor pitch.  
 23 This is done as a function of proton energy for 3 different thicknesses: 1600  $\mu\text{m}$  for 4 SSD as in the overlap  
 24 region of the present prototype, 800  $\mu\text{m}$  for 2 SSD, both for sensors of 400  $\mu\text{m}$  thickness, and 400  $\mu\text{m}$  for 2  
 25 SSD of 200  $\mu\text{m}$  thickness. Also indicated is the angular precision of the intra-telescopes distances  $D = 3, 5,$   
 26 10 cm. At 200 MeV, the largest proton energy at the phantom entrance, the MCS angles of all plane

1 thicknesses approach the intrinsic telescope precision. The angular precision with  $D = 3$  cm exceeds or is  
 2 comparable to the MCS angle for all sensor thicknesses, while the one with  $D=10$  is much smaller than the  
 3 MCS angle. Our choice of  $D=5$  cm, driven by the compactness design goal, will have only a 10% reduction  
 4 in overall angular resolution when compared to  $D=10$  cm. At 80 MeV, the lowest proton energy at the  
 5 phantom exit, the MCS angle exceeds the intrinsic telescope resolution. Therefore we consider using  
 6 thinner sensors of 200  $\mu\text{m}$  thickness (fabricated using the original Fermi mask set) in the first x-y plane of  
 7 the back telescope (X3 in Fig. 2).

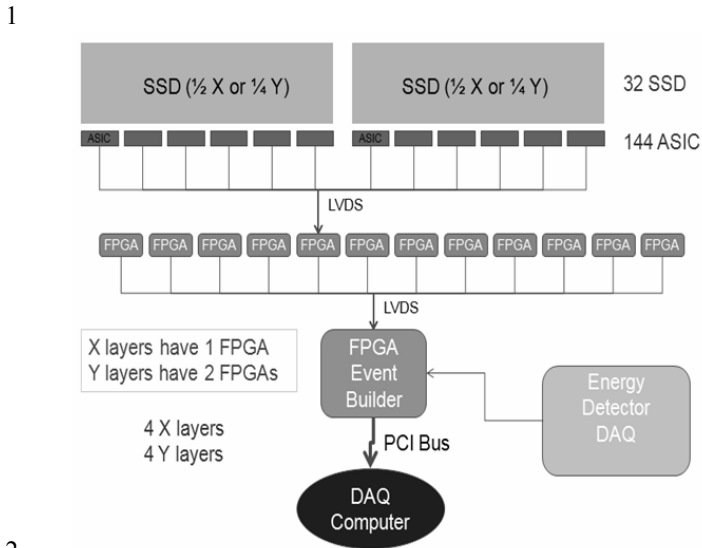


8  
 9 **Fig. 7. MCS angle vs. proton energy, for three thicknesses of one x-y silicon plane. The minimum energy at**  
 10 **the phantom exit is 80 MeV. Also shown are the angular precision of the silicon telescopes for three intra-**  
 11 **telescope distances  $D$ . A typical MCS angle of the phantom is 2-4 degrees.**  
 12

### 13 3.4 Data Flow in the Tracker

14 As mentioned before, increasing the data rate to exceed 2 MHz is the center part of the upgrade toward  
 15 clinical application. Si sensors are intrinsically fast, so the solution is to design a readout ASIC faster than  
 16 the one built for Fermi [13] and a distributed data acquisition (DAQ), employing local FPGAs for data  
 17 collection, formatting and transmission. The concept of the DAQ is shown in Fig. 8. Twelve field  
 18 programmable gate arrays (FPGAs) are needed to acquire the data from the 144 front-end ASICs, which  
 19 read out the 32 single sided silicon strip detectors (SSDs). Twelve serial lines then carry the data from  
 20 those FPGAs to the event builder, which sits on the DAQ computer PCI bus. The tracker data for a single  
 21 proton will consist of about 350 bits. The high speed of the PCI bus allows complete events to flow into  
 22 the computer's memory at the desired rate of at least a million protons per second. All digital signals are  
 23 transmitted on low-voltage differential signal (LVDS) serial lines.

24 A SSD is read out by a 64 channel ASIC, which is being designed specifically for this high rate  
 25 application. Each channel has a two-stage amplifier followed by a discriminator. The shaping time of the  
 26 amplifier has been selected to match the time structure of the proton beam of the Loma Linda University  
 27 Center (LLUMC) synchrotron, which consists of "buckets" 100 ns apart within a much longer spill. Using  
 28 a 200 ns peaking time of the amplifier, all tracker hits can be associated with a specific "bucket". The  
 29 discriminator output is sampled by logic that looks for a rising edge. The resulting short pulses feed into a  
 30 FIFO that holds the data long enough for a trigger decision to be made by the external logic. When the  
 31 trigger is received, the data are transferred from the FIFO into one of four parallel event processors, which  
 32 reduce the 64-channel data into a list of clusters, which is stored in one of four event buffers pending  
 33 readout. A logical OR of all 64 channels is output asynchronously for use by the trigger logic, although we  
 34 expect the main trigger to be done with the energy detector.



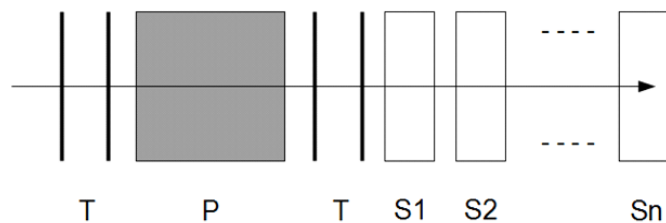
2  
3 **Fig. 8. Data Flow block diagram, showing the distributed FPGAs within the DAQ.**  
4

5 **4 ENERGY/RANGE DETECTOR DESIGN AND R&D**

6 For the required speed of the planned head scanner, the presently used CsI crystals are much too slow as  
7 a calorimeter material. We are planning to use polystyrene scintillator, which is very fast, but has the  
8 disadvantage to be less dense and thus requiring a longer energy detector.  
9

10 **4.1 Water Equivalent Path Length (WEPL)**

11 The integrated S.P. measurement is equivalent to determining the Water Equivalent Path Length (WEPL)  
12 inside the phantom by subtracting the measured residual range from the range of the proton. This can be  
13 done by calibrating the detector with a set of degraders of known Water Equivalent Thickness WET  
14 (density and thickness), and extract the WEPL resolution as a function of the degrader thickness [14]. The  
15 different options to measure WEPL are shown schematically in Fig. 9. The energy/range detector is  
16 indicated by the segments S1 to Sn. A calorimeter consists of only one block ( $n=1$ ), and a range counter  
17 has a large number of plates ( $n \approx 100$ ). A multi-stage detector is a hybrid between the two choices, consisting  
18 of a few blocks ( $n = 3 - 10$ ).  
19



21 **Fig. 9. Schematic of the energy/range detector:  $n=1$ : calorimeter,  $n \approx 100$ : range counter,  $n=few$ : multi-stage**  
22 **detector (T = tracker telescopes, P =phantom).**  
23

24 **4.2 Range Counter with direct SiPM Readout**

25 The main challenge for the S.P. measurement in pCT is range/energy straggling. The straggling  
26 uncertainty is a function of depth, and for a stopping proton amounts to about 1% of the range. Since the

energy loss in the phantom can't be measured directly, straggling in the phantom limits the accuracy of the energy/range measurement. A residual range detector [15] will always encounter the maximum range straggling, independent of the depth of the phantom, since the straggling material in phantom and range counter simply add. Geant4 simulations have shown that for 200 MeV protons, a polystyrene range counter with has almost constant resolution of close to 4 mm for plate thickness between 1 mm and 6 mm. We are pursuing a range counter with 4 mm plates, with direct readout using  $3 \times 3 \text{ mm}^2$  Silicon Photomultipliers (SiPM) and have good initial results using the HPK MCCP S10931-100P, shown on Fig 10. In a 200 MeV proton beam, the signal is 38 photo electrons (p.e.) when derived from the one p.e. signal, and 45 p.e. when derived from the width-to-peak ratio. As indicated in Fig. 10, the high photo electron yield permits a threshold of 5 p.e. without loss of efficiency and with an acceptable dark counting rate of less than 10 kHz.

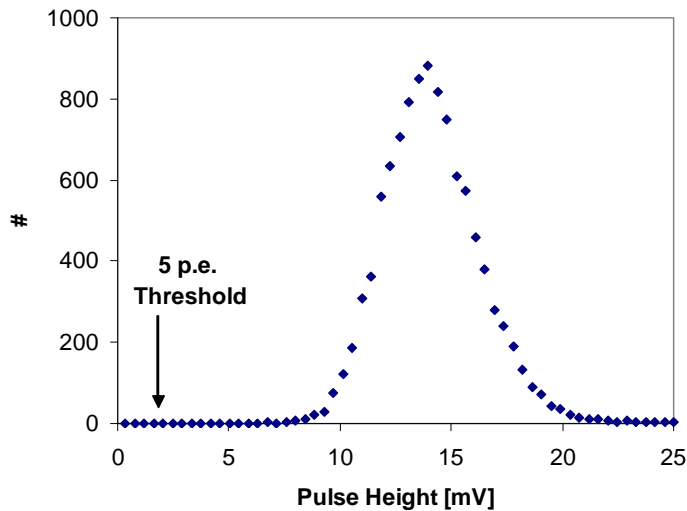


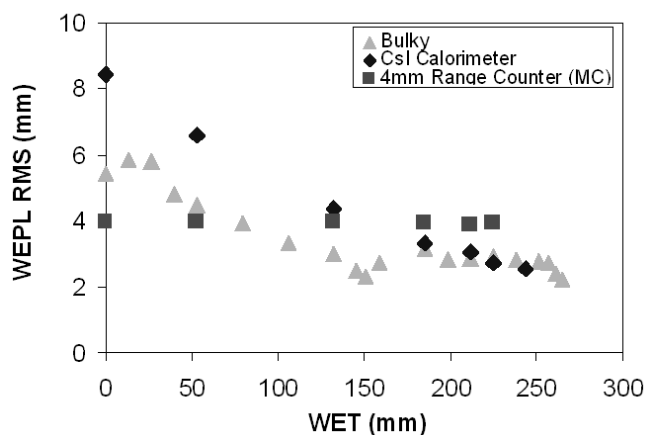
**Fig. 10. Measured pulse height signal of a 4.3 mm thick polystyrene plate with direct SiPM readout in a 200 MeV proton beam. The width of the distribution indicates a photo-electron yield of 45.**

#### 4.3 Multi-Stage WEPL Detector

Because of the straggling limitation of the range detector we are pursuing also a hybrid multi-stage detector, combining coarse range with fine calorimeter measurements. For an initial test, we have implemented a 2-stage hybrid, called “Bulky”, consisting of two polystyrene blocks of 10 cm x 10 cm cross section and 40 cm length read out at the end by 3” photo multiplier tubes (PMT). Obviously, this arrangement does not stop the direct 200 MeV proton beam, but can be used to understand systematic effects in a multi-stage detector. To determine the WEPL, one converts the energy in the block in which the proton stops to WET and adds, if applicable, the WET of the block in front. Thus the energy which is measured is generally smaller than if measured in a calorimeter and thus has a smaller error.

A WEPL calibration of the 2-stage “Bulky” was performed in the 200 MeV proton beam of the LLUMC synchrotron, using degraders as described above. The initial results on its WEPL resolution as a function of degrader thickness WET are shown in Fig. 11, comparing “Bulky”, the CsI calorimeter of our present prototype [5, 14], and a Monte Carlo simulation of a range counter with 4 mm polystyrene plates. The 2-stage hybrid performs better than the CsI calorimeter over the entire WET range, and its resolution is about 40% lower than the range detector. A 3-stage “Bulky” under construction would improve the data below  $\text{WET} = 50 \text{ mm}$ , since it would be measured with the proton stopping in the 3<sup>rd</sup> stage, while it is now measured in the 2<sup>nd</sup> stage in transmission as  $dE/dx$ . An obvious drawback of this hybrid multi-stage

1 detector with respect to a range detector is the need for continuous careful calibration, which would be a  
 2 waste of proton beam time, and possible interference of magnetic fields in the gantry.



3  
 4 **Fig. 11. Comparison of the measured WEPL resolution for a CsI calorimeter [5, 14] and a 2-stage “Bulky”**  
 5 **detector and the simulated WEPL RMS of a range counter with 4 mm polystyrene plates. The “Bulky”**  
 6 **resolution is expected to improve below WET = 50 mm for a 3-stage detector.**  
 7

## 8 5 CONCLUSIONS

9 We are now arriving at a new phase in pCT with a dedicated detector development of a large-area  
 10 scanner with data acquisition speed useful in clinical applications.

11 The most advanced R&D topics are slim edges for the silicon sensors of the tracking system, a hybrid  
 12 multi-stage WEPL detector for the energy/range detector and a data acquisition system sustaining 2 MHz  
 13 proton rate.

14 End-to-end simulation of the instrument has been essential for our understanding of the requirements and  
 15 proper choice of the technical solution, yet many lessons were learned during operation of the existing  
 16 prototype and reconstruction of the data.

17 The next crucial step will be technology transfer into a hospital environment and development of clinical  
 18 testing protocols.

## 19 ACKNOWLEDGMENTS

20 Ongoing and unwavering support by Prof. James M. Slater (LLUMC) made this project possible.

21 The project described was supported by Award Number R01EB013118 from the National Institute of  
 22 Biomedical Imaging And Bioengineering (NIBIB). The content is solely the responsibility of the authors  
 23 and does not necessarily represent the official views of the National Institute of Biomedical Imaging And  
 24 Bioengineering or the National Institutes of Health.

## 25 REFERENCES

- 26 [1] H. F.-W. Sadrozinski et al., “Toward Proton Computed Tomography”, *IEEE Trans. Nucl. Sci.*, vol 51,  
 27 3, 2004.  
 28 [2] R. Schulte et al., “Conceptual design of a proton computed tomography system for applications in  
 29 proton radiation therapy”, *IEEE Trans. Nucl. Sci.*, vol 51, 866, 2004.  
 30 [3] D. C. Williams, “The most likely path of an energetic charged particle through a uniform medium”.  
 31 *Phys. Med. Biol.* 49 (2004) 2899.  
 32 [4] M. Bruzzi et al., “Prototype Tracking Studies for Proton CT”, *IEEE Trans. Nucl. Sci.*, vol 54, 140,  
 33 2007.

- 1 [5] H. F.-W. Sadrozinski et al. "Detector Development for pCT", Conference Record, 2011 IEEE NSS-  
2 MIC Conference, 4457.
- 3 [6] S. Penfold, "Image Reconstruction and Monte Carlo Simulations in the Development of Proton  
4 Computed Tomography for Applications in Proton Radiation Therapy", PhD thesis Univ. of  
5 Wollongong, 2010.
- 6 [7] M. Petterson et al., "Proton Radiography Studies for Proton CT", Conference Record, 2006 IEEE NSS-  
7 MIC Conference, 2276.
- 8 [8] M. Petterson, "Resolution of a PMMA Phantom using 200 MeV Protons", UC Santa Cruz Physics  
9 Department Senior Thesis, June 23, 2006.
- 10 [9] G. Herman, "Fundamentals of Computerized Tomography, Image Reconstruction from Projections";  
11 Springer Verlag, N.Y., 2<sup>nd</sup> edition, (2009), p. 56.
- 12 [10] T. Ohsugi et al., "Design and properties of the GLAST flight silicon micro-strip sensors", Nucl. Instr.  
13 Meth. A 541 (2005) 29.
- 14 [11] M. Christophersen et al., "Alumina and Silicon Oxide/Nitride Sidewall Passivation for P- and N-Type  
15 Sensors", these Proceedings.
- 16 [12] R. Mori et al., "Charge collection measurements on slim-edge microstrip detectors", SCIPP 12/02, to  
17 be published in Journal of Instrumentation JINST.
- 18 [13] R.P. Johnson et al., "An amplifier-discriminator chip for the GLAST silicon-strip tracker", *IEEE*  
19 *Trans. Nucl. Sci.*, vol 45, 927, 1998.
- 20 [14] R. F. Hurley et al., "Water-Equivalent Path Length Calibration of a Prototype Proton CT Scanner", to  
21 be published in Medical Physics, 2011.
- 22 [15] U. Amaldi et al., "Construction, test and operation of a proton range radiography system" Nucl. Instr.  
23 Meth. A629 (2011) 337.
- 24